Design and Modeling of Flexible Passive Rowing Joint for Robotic Fish Pectoral Fins

Sanaz Bazaz Behbahani, *Student Member, IEEE*, and Xiaobo Tan, *Senior Member, IEEE*

***Abstract*—Paired pectoral fins that are capable of rowing motions are an important actuation mechanism for robotic fish. Existing work in this area typically adopts a rigid connection between the actuator and the pectoral fins, which requires a faster actuation speed in the power stroke than in the recovery stroke to produce a net thrust or moment. In addition to increasing the control complexity, the latter requirement leads to slow robot speeds due to prolonged deceleration during the recovery stroke. In this paper, we propose the design of a novel flexible passive joint that connects the servomotor arm to the pectoral fin, to overcome the aforementioned problem. A dynamic model is developed for the joint and for a robotic fish equipped with such joints. The design and the model are evaluated with extensive experimental results. With symmetric actuation patterns during the power and recovery strokes, the robotic fish with the proposed joints shows clear speed advantage over the case involving rigid joints and asymmetric actuation. Motivated by the need for design optimization, the model is further utilized to investigate the influence of the joint length and stiffness on the robot locomotion performance and efficiency. It is found that, for low fin-beat frequencies, longer or more flexible joints lead to higher speeds, and the trend is reversed at high fin-beat frequencies. On the other hand, while the mechanical efficiency shows a decreasing trend when the frequency increases, it is higher with shorter joints. These findings suggest the utility of the proposed model for multiobjective design of the joint and its operating frequency.**

***Index Terms*—Blade element theory, dynamic model, efficiency, labriform locomotion, pectoral fins, robotic fish.**

I. Introduction

UNDERWATER creatures, especially fish, have fascinating swimming abilities and behaviors, which have motivated tremendous interest in fish-like underwater robots, often known as robotic fish. Fish swimming has been studied extensively for decades [1]–[4]. The understanding of fish locomotion and maneuvering has inspired various designs of robotic fish [5]–[8]. Fish-like robots are expected to be more efficient, stealthy, and maneuverable than traditional underwater vehicles [9]. Robotic fish have a wide range of applications, examples of which include monitoring aquatic environments [10], [11] and serving as a tool for studying the locomotion and social behavior of live fish [12].

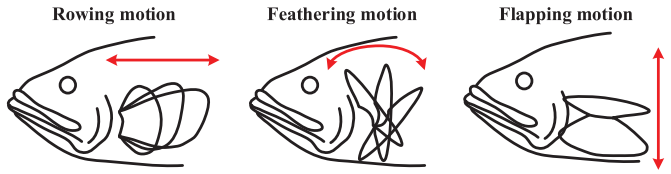

Fig. 1. Types of pectoral fin motion (Adapted from [33]). The rotation axes for the rowing, feathering, and flapping motions are vertical, transverse, and longitudinal, respectively.

Robotic fish can be actuated in many different ways, which, inspired by live fish motion, all involve deforming the body and/or moving the fins [13]–[17]. The latter can be done by utilizing motors [18]–[20], or smart materials [21]–[25]. Work has also been reported on fins with tunable stiffness for optimization of propulsion performance [26]–[30]. One of the swimming modes that a live fish often uses in maneuvering and assistive propulsion is the "labriform" swimming mode, in which the fish oscillates its paired pectoral fins to generate thrust [3], [4]. Previous works done on a robotic fish actuated by paired pectoral fins include both rigid pectoral fins [31]–[35] and flexible fins or fins with controlled curvature [36]–[39]. As illustrated in Fig. 1, pectoral fin motions can generally be classified into three modes based on the axis of rotation, rowing, feathering, and flapping. The feathering motion represents fin rotation about the transverse axis, and in robotic fish, feathering pectoral fins have often been used as bow planes to control the dive and ascent of the robots [31], [40], [41]. The flapping motion involves fin rotation about the longitudinal axis, which has been used in several robotic manta rays involving expanded flexible pectoral fins [42], [43]. Finally, the rowing motion involves fin rotation about the vertical axis, which can be utilized for a number of in-plane locomotion and maneuvering tasks, such as forward swimming, sideway swimming, and turning [44].

The fin-beat cycle in the rowing motion involves a power stroke, where the fin rotates toward the back of the robot and gains thrust via the induced-drag on the fin, and a recovery stroke, where the fin rotates back toward the front of the body and gets ready for the next cycle. In order to generate a net thrust over each cycle, the fin has to be actuated differently in the power and recovery strokes. For example, one can actuate the fin (much) faster in the power stroke than in the recovery stroke [38]. The downside of this approach, however, is that the robot will decelerate and lose momentum during the extended recovery stroke and the resulting robot motion is slow. An alternative approach is to feather the fin to reduce its effective area and,

Manuscript received September 21, 2015; revised April 15, 2016; accepted August 8, 2016. Date of publication September 14, 2016; date of current version September 30, 2016. This paper was recommended for publication by Associate Editor F. Boyer and Editor A. Billard upon evaluation of the reviewers' comments. This work was supported in part by the National Science Foundation under Grant DBI-0939454, Grant CNS-1059373, Grant IIP 1343413, and Grant IIS-1319602.

The authors are with the Smart Microsystems Laboratory, Department of Electrical and Computer Engineering, Michigan State University, East Lansing, MI 48824 USA (e-mail: bazazbeh@msu.edu; xbtan@msu.edu).

Color versions of one or more of the figures in this paper are available online at http://ieeexplore.ieee.org.

Digital Object Identifier 10.1109/TRO.2016.2593452

thus, drag during the recovery stroke [19], [34], [44]. The latter, however, entails the need of one additional actuator for each pectoral fin, which significantly increases the size, weight, and complexity of the fins and the overall robot.

The contribution of this paper is the proposal and modeling of a flexible, passive joint for a pectoral fin that enables net thrust generation under symmetric actuation of a single rowing actuator in power and recovery strokes. The proposed design has significantly reduced complexity and cost comparing to the approach adopting active feathering, and as demonstrated later in the paper, it results in superior swimming performance comparing to the case of a single actuator with a rigid link and differential power/recovery actuation. The flexible joint allows the pectoral fin to sweep back passively during the recovery stroke, while following the motion prescribed by the actuator during the power stroke. Consequently, the fin experiences less drag in the recovery stroke than in the power stroke, resulting in a net thrust. To analyze the robot locomotion performance, a dynamic model is developed for the joint and fin structure and for a robotic fish equipped with a pair of such pectoral fins. This model is then validated by performing experiments on a free-swimming robotic fish. Experiments are also conducted to compare the robot performance using the flexible joint with the case where a rigid joint is used. The model is further exploited to investigate the effect of length and stiffness of the flexible joint on the robotic fish swimming performance at different fin-beat frequencies. Joint structures of different length and stiffness values are prototyped with a multimaterial 3-D printer to confirm the model analysis. Finally, the mechanical efficiency for a given flexible joint design is computed, which, along with the swimming performance analysis, offers an instrumental tool for multiobjective optimization of the fin joint and its operating frequency.

A preliminary version of this work was presented at the 2014 IROS conference [45]. The improvement of this paper over [45] includes the following. First, on the experimental side, data reported here were collected with a new robotic fish prototype using an enhanced experimental setup (for example, robot trajectories were captured and extracted with an OptiTrak system, while in [45], the measurements were conducted manually). In addition, additional experiments were carried out on the robotic fish in an anchored configuration, to capture the images of fin joints during actuation for model validation (see Figs. 11 and 12). Most, if not all, figures involving data in this paper are different from those in [45]. Second, the analysis of mechanical efficiency was not included in [45]. Finally, the writing has been polished throughout the paper.

The remainder of this paper is organized as follows. The design and prototyping of the flexible rowing joint are described in detail in Section II. Section III presents the dynamic model for the joint structure along with the model for robotic fish adopting such joints for pectoral fins. Blade element theory is used to calculate the hydrodynamic forces on the pectoral fins, and the flexible rowing joint is modeled as a pair of torsional spring and damper. In Section IV, experimental results are provided to support the modeling analysis. The effect of the flexible joint length and stiffness is investigated in Section V. The mechanical efficiency of robotic fish adopting a given design of the pectoral fin joint is derived and explored numerically in Section VI. Finally, concluding remarks are provided in Section VII.

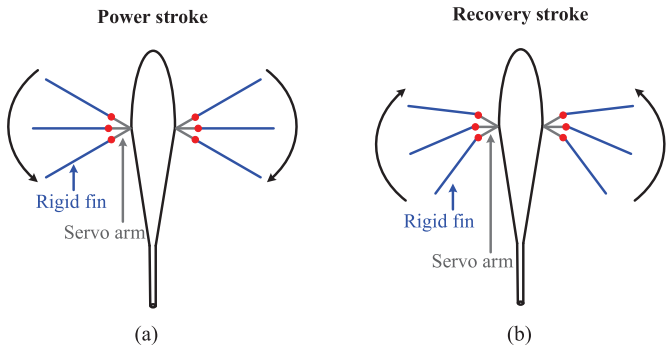

Fig. 2. Illustration of the motion of the pectoral fins with flexible rowing joints (top view): (a) Power stroke, (b) recovery stroke. The flexible joints are marked with red dots.

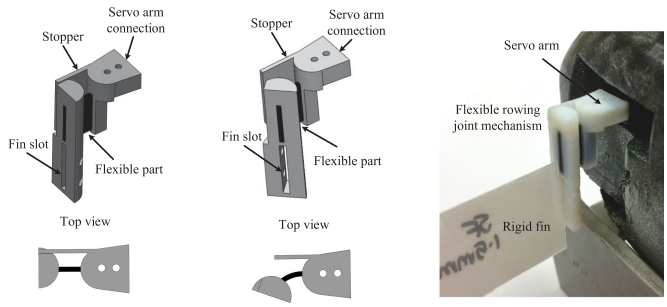

Fig. 3. Proposed flexible rowing joint designed in SolidWorks software: (a) During the power stroke, the mechanical stopper prevents the fin from sweeping forward passively (which would reduce thrust), (b) during the recovery stroke, the fin bends back passively under the hydrodynamic forces, which reduces the drag on the fin and thus on the robot, and (c) 3D-printed rowing passive joint assembled on the robotic fish.

II. Joint Design

This section is dedicated to describing the design and prototyping of the proposed flexible rowing joint. Each pectoral fin moves back and forth utilizing a servo motor as the source of actuation. In fish locomotion, the main target is to maximize the overall thrust force and minimize the hydrodynamic drag force in the recovery stroke [3]. To meet this goal for a robotic fish, the flexible rowing joint is designed such that the pectoral fin maintains the motion prescribed by the servo in the power stroke, to produce the maximum thrust, while sweeping back passively along the body in the recovery stroke, to minimize the drag force on the fin. Fig. 2(a) and (b) illustrates the motion of the pectoral fins with the flexible rowing joints during the power and recovery strokes, respectively. One can see that, in this case, the fin plane stays vertical throughout the stroke cycle and, thus, the resulting hydrodynamic force is restricted to the horizontal plane. SolidWorks software is used to design the passive joints, which is shown in Fig. 3. The entire joint assembly consists of four parts:

1) A rigid servo arm connection that will fit to the servo arm,
2) A mechanical stopper rigidly attached to the servo arm connection,

TABLE I
SPECIFICATIONS OF FOUR DIFFERENT FLEXIBLE ROWING JOINTS

Joint name	Flexible part material	Flexible part length (mm)
JR1	FLX980	0.5
JR2	FLX980	1
JR3	FLX980	1.5
JR4	DM9850	0.5

3) A fin mount (rigid) with a slit for attaching the pectoral fin,
4) A piece of flexible material with a rectangular shape, serving as the joint between the servo arm connection and the fin mount.

The stopper is designed to prevent the pectoral fin from sweeping forward passively and let it follow the prescribed servo motion, during the power stroke, as illustrated in Figs. 2(a) and 3(a), while allowing the fin to sweep back passively during the recovery stroke, as illustrated in Figs. 2(b) and 3(b).

The joint is prototyped using a multi-material 3-D printer (Connex 350 from Objet). The printer is capable of simultaneously jetting rigid and flexible materials, so the entire joint structure is printed seamlessly as a single piece, as shown in Fig. 3(c). All the rigid parts are printed with RGD835 (VeroWhitePlus). Two different materials, FLX980 (TangoBlackPlus), which is the most flexible material from the printer, and DM9850 (Digital Material 9850), which is still flexible but stiffer than the former, are explored for the flexible part of the joint structure. Other than different stiffnesses for the flexible part, we aim to investigate the effect of joint dimension on the performance of the fish as well. To do so, four different joints are printed, three using FLX980 and one using DM9850. All the joints have fixed depth and thickness of 10 and 1 mm, respectively, to ensure the joints survive through extensive experiments. Table I summarizes the specifications of all four joints.

III. DYNAMIC MODELING

One of the main foci of this study is to analyze and compare the passive joint mechanism with a traditional rigid joint. For this purpose, we have developed a dynamic model for robotic fish propelled with pectoral fins, for the case involving flexible and passive rowing joints. The fluid that the robotic fish operates in is considered to be inviscid and incompressible. The robot is assumed to have a rigid body with a pair of rigid pectoral fins, which are coupled to the actuator arms through the proposed flexible joints. While one can incorporate an active caudal fin for the robotic fish, as we did for our prototype reported in this paper, its modeling and study are outside the scope of this paper. The blade element theory [3] is used to evaluate the hydrodynamic forces generated by the pectoral fins.

A. Rigid Body Dynamics

To model the robotic fish motion properly, some coordinate systems need to be defined. As illustrated in Fig. 4, the inertial

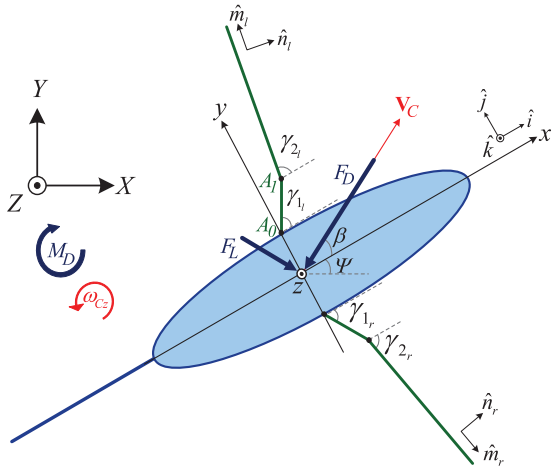

Fig. 4. Top view of the robotic fish actuated by pectoral fins in a planar motion.

coordinate system is denoted with $[X, Y, Z]$, and the body-fixed coordinate system is represented by $[x, y, z]$, with the corresponding unit vectors denoted by $[\hat{i}, \hat{j}, \hat{k}]$, which is attached to the center of mass of the robotic fish. Here the x-axis is along the body's longitudinal axis pointing to the head, the z-axis is perpendicular to the x-axis and points upward, and the y-axis is automatically formed by the right-hand orthonormal principle. We denote by $\vec{r}_{c_p} = c_p\hat{j}$ the vector pointing from robotic fish center of mass to the base of the pectoral fin servomotor (point A_0). Point A_1 is the base of the pectoral fin. We use $\hat{m}$ and $\hat{n}$ to denote the unit vectors parallel and perpendicular, respectively, to each pectoral fin, where subscripts r and l are used to denote the right and left fins, respectively. The robotic fish is considered to be neutrally buoyant. Let $\mathbf{V}_C = [V_{C_x}, V_{C_y}, V_{C_z}]^T$ denote the velocity vector of the robotic fish in the body-fixed coordinates, where V_{C_x}, V_{C_y}, and V_{C_z} are the surge, sway, and heave components, respectively. On the other hand, $\boldsymbol{\omega}_C = [\omega_{C_x}, \omega_{C_y}, \omega_{C_z}]^T$ denotes the body-fixed angular velocity vector of the body, where ω_{C_x}, ω_{C_y}, and ω_{C_z} are the roll, pitch, and yaw components, respectively. We use γ_1 and γ_2, along with subscripts r and l, to denote the angle of the servo, and deflection angle of each pectoral fin with respect to the x-axis, respectively. The angle of attack for the body is denoted as β, which is the angle between the x-direction of the body-fixed coordinate system and the velocity vector $\mathbf{V}_C$. Finally, let ψ denote the angle between the x-axis and X-axis.

The rigid body dynamics in the body-fixed coordinates are represented as [46]

$$\begin{bmatrix} \mathbf{m} & 0 \\ 0 & \mathbf{I} \end{bmatrix} \begin{bmatrix} \dot{\mathbf{V}}_C \\ \dot{\omega}_C \end{bmatrix} + \begin{bmatrix} \omega_C \times \mathbf{m}\mathbf{V}_C \\ \omega_C \times \mathbf{I}\omega_C \end{bmatrix} = \begin{bmatrix} \mathbf{f} \\ \tau \end{bmatrix} \tag{1}$$

where $\mathbf{m}$ is the mass matrix (incorporating both the actual robot mass and the added mass, which is calculated considering an ellipsoid accelerating in the fluid [47]), $\mathbf{I}$ is the inertia matrix (including both the actual and added inertias), $\mathbf{f} = [f_x, f_y, f_z]^T$ represents the external hydrodynamic forces, $\tau = [\tau_x, \tau_y, \tau_z]^T$ represents the external moments, applied to the center of mass of the robotic fish, and "$\times$" denotes the vector product.

In this paper, we focus on the planar motion for the robotic fish, so it has three degrees of freedom, namely, surge (V_{C_x}), sway (V_{C_y}), and yaw (ω_{C_z}). We further assume that the body is symmetric with respect to the xz-plane, the pectoral fins move in the xy-plane, and the z-axis of the body-fixed frame is parallel to the z-axis of the inertial frame. The inertial couplings between these three states are assumed to be negligible [23], which simplifies (1) to

$$(m_b - m_{a_x})\dot{V}_{C_x} = (m_b - m_{a_y})V_{C_y}\omega_{C_z} + f_x \tag{2}$$

$$(m_b - m_{a_y})\dot{V}_{C_y} = -(m_b - m_{a_x})V_{C_x}\omega_{C_z} + f_y \tag{3}$$

$$(I_z - I_{a_z})\dot{\omega}_{C_z} = \tau_z \tag{4}$$

where m_b is the robotic fish mass, $-m_{a_x}$ and $-m_{a_y}$ are the added mass components along the x- and y-directions of the body-fixed coordinates, respectively. I_z is the robot inertia about the z-axis, and $-I_{a_z}$ is the added inertia of the robot about the same axis. The variables f_x, f_y, and τ_z denote the external hydrodynamic forces and moment exerted on the fish body, which are described as

$$f_x = F_{h_x} - F_D \cos\ \beta + F_L \sin\ \beta \tag{5}$$

$$f_y = F_{h_y} - F_D \sin\ \beta - F_L \cos\ \beta \tag{6}$$

$$\tau_z = M_{h_z} + M_D \tag{7}$$

where F_{h_x}, F_{h_y}, and M_{h_z} are the hydrodynamic forces and moment transmitted to the fish body by the pectoral fins and the calculation procedure is addressed in detail in Section III-B. F_D, F_L, and M_D are the body drag, lift, and moment, respectively. These forces and moment are expressed as [23], [31], [48]

$$F_D = \frac{1}{2}\rho V_C^2 S_A C_D \tag{8}$$

$$F_L = \frac{1}{2}\rho V_C^2 S_A C_L \beta \tag{9}$$

$$M_D = -C_M \omega_{C_z}^2\ \mathrm{sgn}(\omega_{C_z}) \tag{10}$$

where V_C is the linear velocity magnitude of the robotic fish body, $V_C = \sqrt{V_{C_x}^2 + V_{C_y}^2}$, ρ is the mass density of water, S_A is the wetted area of the body, C_D, C_L, and C_M are the dimensionless drag, lift, and damping moment coefficients, respectively, and sgn(.) is the signum function.

Finally, the kinematics of the robotic fish is described as [48]

$$\dot{X} = V_{C_x}\ \cos\ \psi - V_{C_y}\ \sin\ \psi \tag{11}$$

$$\dot{Y} = V_{C_y}\ \cos\ \psi + V_{C_x}\ \sin\ \psi \tag{12}$$

$$\dot{\psi} = \omega_{C_z}. \tag{13}$$

B. Hydrodynamic Forces From Pectoral Fins With Flexible Rowing Joints

In this section, we present the detailed model for computing the hydrodynamic forces generated by the pectoral fins. First, we introduce the blade element theory that is used to evaluate the hydrodynamic forces and moment for a given fin movement. We then describe the dynamic model of the pectoral fins under the proposed flexible joints, which enable the computation of the corresponding hydrodynamic forces and moment for a prescribed servo motion.

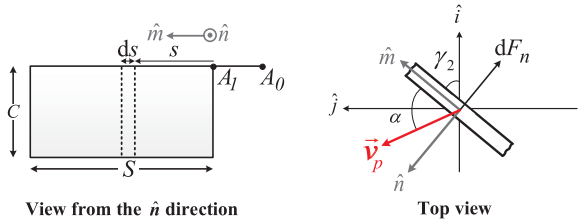

Fig. 5. Illustration of a rigid, rectangular pectoral fin and its parameters and variables.

1) Blade Element Theory: Following [3], the blade element theory is used to evaluate the hydrodynamic forces on the pectoral fins. For ease of calculations, the pectoral fin is considered to be rectangular with span length S and chord length (depth) C, as illustrated in Fig. 5. The following calculation uses the left pectoral fin as an example, but it will extend trivially to the right pectoral fin.

The relationship between the unit vectors $\hat{m}$ and $\hat{n}$, and the body-fixed coordinates is given by

$$\hat{m} = \cos\gamma_{2_l}\ \hat{i} + \sin\gamma_{2_l}\ \hat{j} \tag{14}$$

$$\hat{n} = -\sin\gamma_{2_l}\ \hat{i} + \cos\gamma_{2_l}\ \hat{j}. \tag{15}$$

The hydrodynamic forces on the pectoral fin have span-wise and normal components. Since the pectoral fins are considered to have pure rowing motion in this study, the angle between the pectoral fin and the flow is large, which results in a very small span-wise force, which arises from friction, and can be neglected [49]. In blade element theory, the normal force $\mathrm{d}F_n(s,t)$ is calculated on each defined blade element, $\mathrm{d}s$, at time t

$$\mathrm{d}F_n(s,t) = \frac{1}{2}C_n \rho C |\vec{v}_p(s,t)|^2 \mathrm{d}s \tag{16}$$

where $\vec{v}_p(s,t)$ is the velocity of each blade element of the pectoral fin as a result of both the robot body motion and the pectoral fin motion, and C_n is the normal force coefficient, which depends on the angle of attack of each arbitrary blade, $\alpha(s,t)$. Utilizing a model empirically evaluated for insect wings and assuming that its validity holds underwater [47], $C_n = 3.4\sin\alpha$. The details on calculating the angle of attack for the fin is presented in Section III-B2. The total hydrodynamic force acting on each pectoral fin is calculated by integrating the force density along the span length of the fin

$$F_n(t) = \int_0^S \mathrm{d}F_n(s,t)\ . \tag{17}$$

2) Modeling of the Flexible Joint: The motion of the fin in both power and recovery strokes should be known, in order to utilize blade element theory to calculate the hydrodynamic forces. To do so, the flexible rowing joint is modeled as a couple of torsional spring and damper, where the parameters are derived from the properties of the flexible part and its dimensions. We consider the servo arm and the rigid pectoral fin as two links,

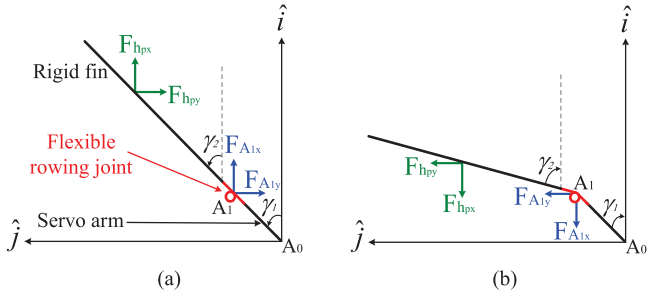

Fig. 6. Dynamic configuration of the pectoral fin with flexible rowing joint during: (a) Power stroke, and (b) recovery stroke. A_1 represents the flexible joint.

which are connected by the flexible rowing joint. We denote the angles made by the first and second links with respect to the x-axis as γ_1 and γ_2, respectively. As illustrated in Fig. 6(a), during the power stroke, the angle γ_1 is dictated by the servo and the fin follows the prescribed motion of the servo arm, resulting in $\gamma_2 = \gamma_1$, so the trajectory of the pectoral fin is fully known. On the other hand, for the recovery stroke, the motion of each point on the rigid fin is determined by the hydrodynamic interactions, as shown in Fig. 6(b). Therefore, we need to find the angle of the second link, γ_2, in order to compute the motion of each point on the fin.

Refer to Fig. 4. Velocities of the point A_0 (base of the servomotor) and point A_1 (base of the pectoral fin) in the inertial frame can be expressed as

$$\vec{v}_{A_0}(t) = \left\{V_{C_x} - c_p\omega_{C_z}\right\}\ \hat{i} + \left\{V_{C_y}\right\}\ \hat{j} \tag{18}$$

$$\vec{v}_{A_1}(t) = \vec{v}_{A_0} - \left\{l_1(\dot{\gamma}_1 + \omega_{C_z})\sin\gamma_1\right\}\ \hat{i} + \left\{l_1(\dot{\gamma}_1 + \omega_{C_z})\cos\gamma_1\right\}\ \hat{j} \tag{19}$$

where c_p is the distance from the body center to point A_0, and l_1 is the length of the servo arm. The velocity at each point s along the pectoral fin is

$$\begin{aligned}\vec{v}_p(s,t) &= \vec{v}_{A_1} - \left\{s(\dot{\gamma}_2 + \omega_{C_z})\sin\gamma_2\right\}\ \hat{i} \\ &\quad + \left\{s(\dot{\gamma}_2 + \omega_{C_z})\cos\gamma_2\right\}\ \hat{j} \\ &= v_{px}\ \hat{i} + v_{py}\ \hat{j}.\end{aligned} \tag{20}$$

The angle of attack of each blade element is calculated via

$$\tan\alpha = \frac{\langle v_p(s,t), \hat{n}\rangle}{\langle v_p(s,t), \hat{m}\rangle} = \frac{-v_{px}\sin\gamma_2 + v_{py}\cos\gamma_2}{v_{px}\cos\gamma_2 + v_{py}\sin\gamma_2} \tag{21}$$

where $\langle\cdot,\cdot\rangle$ denotes the inner product, v_{px} and v_{py} are the velocity of the pectoral fin in x- and y-direction, respectively. The total force acting on the rigid pectoral fin is

$$\vec{F}_2 = \vec{F}_n - \vec{F}_{A_1} = m_p \frac{\mathrm{d}\vec{v}_p(s,t)}{\mathrm{d}t}\bigg|_{s=\frac{S}{2}} \tag{22}$$

where $\vec{F}_{A_1}$ represents the force applied by the rigid pectoral fin on the servo arm, and m_p is the effective mass of the rigid fin (which contains the fin mass and the added mass, where the added mass is calculated based on a rigid plate moving in the water) [50].

The moment of the rigid fin relative to its pivot point (point A_1) is evaluated as

$$\vec{M}_n = \int_0^S s\hat{m} \times \mathrm{d}F_n. \tag{23}$$

Note that $\vec{M}_n$ is a function of γ_2 and $\dot{\gamma}_2$. The moment produced by the torsional spring and damper (namely, the flexible joint itself) is evaluated as

$$\vec{M}_{(S+D)} = [K_S(\gamma_1 - \gamma_2) + K_D(\dot{\gamma}_1 - \dot{\gamma}_2)]\hat{k} \tag{24}$$

where K_S and K_D are the spring and damper coefficients used to model the flexible rowing joint.

The total moment equation of the rigid fin relative to point A_1 is written as

$$\vec{M}_2 = \vec{M}_n + \vec{M}_{(S+D)} = I_p(\ddot{\gamma}_2 + \dot{\omega}_{C_z}) \tag{25}$$

where I_p is the effective inertia of the rigid fin (which contains the fin inertia and the added inertia, and is calculated base on a rigid plate moving in the water) and $\ddot{\gamma}_2$ is the angular acceleration of the second link. By solving (25), which is a second-order equation for γ_2, the dynamics of the pectoral fin with a flexible joint in the recovery stroke is fully described.

The hydrodynamic force transmitted to the servo arm can be obtained as $\vec{F}_{A_1} = F_n\hat{n} - m_p\frac{\mathrm{d}\vec{v}_p(s,t)}{\mathrm{d}t}$, where $\frac{\mathrm{d}\vec{v}_p(s,t)}{\mathrm{d}t}$ can be evaluated once γ_2 and $\dot{\gamma}_2$ are solved from (25). The total force exerted by the arm on the robot body is

$$\vec{F}_h = F_{h_x}\hat{i} + F_{h_y}\hat{j} = \vec{F}_{A_1}. \tag{26}$$

The moment applied by the fin on the body is represented as

$$\vec{M}_h = M_{h_z}\hat{k} = c_p\hat{j} \times \vec{F}_{A_1}. \tag{27}$$

By substituting (26), (27) into (5)–(7), the dynamics of the robotic fish utilizing flexible rowing joints are fully described.

The presented model applies to the case where the robotic fish is free-swimming. The coupled body and fin motions introduce significant complexity in evaluating the fin-generated hydrodynamic force and moment. Alternatively, one could assume an anchored robot body when evaluating the fin-produced force and moment, as often adopted in the literature for similar problems [6], [48], [51]. While the latter simplification, also adopted in the simulation part of this paper, introduces modeling error, the error is typically acceptable considering the much larger fin velocity comparing to the velocity of the robot itself.

IV. Experimental Model Validation

A. Robotic Fish Prototype and Experimental Setup

To evaluate the proposed flexible rowing joint mechanism and validate the presented dynamic model, we conduct experiments on a free-swimming robotic fish prototype. The robot is designed to swim on the surface and is slightly positive buoyant with about 15% of its height above water (as opposed to the neutrally buoyant assumption for dynamic modeling). Due to the relatively slow pectoral fin-actuated locomotion, the effect

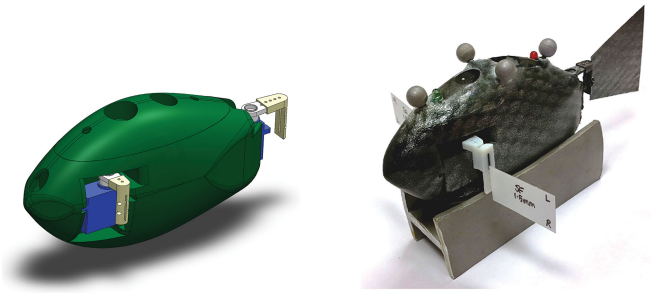

(a) (b)

Fig. 7. Robotic fish prototype: (a) Designed SolidWorks model; (b) 3D-printed robotic fish body along with mounted fins.

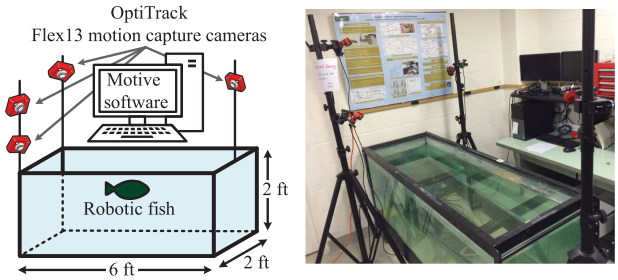

(a) (b)

Fig. 8. Experimental setup: (a) Schematic; (b) actual.

of tank walls and surface waves is contemplated to be negligible in this study. The body of the robotic fish is designed in SolidWorks and 3D-printed. Both the design schematic and the actual prototype are shown in Fig. 7. This prototype is about 15 cm long, 8 cm high, and 4.6 cm wide without the pectoral and caudal fins, and weighs close to 0.3 kg. The robotic fish utilizes a pro mini microcontroller board from Arduino to realize the control of the three servos. A power converter printed circuit board is specifically designed for this robotic fish. Three waterproof servos (Traxxas 2065) are utilized to actuate the fins, although tail actuation is not included in this study. The servomotors are programed to rotate each pectoral fin according to

$$\gamma_1(t) = \gamma_A \sin(\omega_\gamma t) + 90^\circ \tag{28}$$

with γ_A and ω_γ denoting the amplitude (in degree) and the angular frequency of fin actuation, respectively. The actual pectoral fins are made of a polypropylene sheet with 0.5 mm thickness and Young's modulus of approximately 2 GPa, which is considered to be almost rigid.

The experiments are conducted in a tank that measures 2 feet wide, 6 feet long, and 2 feet deep. The tank is equipped with a motion capture system from NaturalPoint, which contains four Optitrack Flex 13 cameras along with the Motive software to capture the motion of the robotic fish. The experimental setup is shown in Fig. 8. Two types of experiments, forward swimming and turning, are performed to evaluate the dynamic model. We let the robotic fish swim for some time (approximately 30 s) to reach the steady-state motion, and then video-tape its swimming. For example, in the forward swimming case, we record the time

TABLE II
IDENTIFIED MODEL PARAMETERS

Component	Parameter	Value	Unit
Body	Mass (m_b)	0.295	Kg
	Inertia (I_z)	4.26×10^{-4}	Kg/m^2
	$-m_{a_x}$	0.095	Kg
	$-m_{a_y}$	0.1794	Kg
	$-I_{a_z}$	2.7×10^{-5}	Kg/m^2
	Wet surface area (S_A)	0.0325	m^2
	Drag coef. (C_D)	0.42	–
	Lift coef. (C_L)	4.86	–
	Moment coef. (C_M)	7.6×10^{-4}	Kg/m^2
Fin	Length (S)	0.043	m
	Depth (C)	0.025	m
	Servo arm length (l_1)	0.01	m
	Effective mass (m_p)	0.0194	Kg
	Effective inertia (I_p)	3.49×10^{-6}	Kg/m^2
	Distance from body center c_p to servo base,	0.025	m
	Water density (ρ)	1000	Kg/m^3

it takes for the robot to swim a distance of 50 cm. The experiment for each setting is repeated ten times. Finally, we analyze the captured videos to extract the steady-state speed for the forward swimming, and turning radius and period for the turning motion.

B. Parameter Identification

The parameters for the dynamic model are measured directly or calculated based on measurements and are listed in Table II. The body inertia about z-axis is evaluated as $I_z = \frac{1}{5} m_b (a^2 + c^2)$, where $a = \frac{\text{Body length}}{2}$ and $c = \frac{\text{Body width}}{2}$ are the semiaxis lengths [23]. Even though the robotic fish body (with all its internal components) is not homogeneous, later experimental results show that the aforementioned inertia formula produces a satisfactory approximation to the reality. The wet surface area, added masses, and added inertia are calculated considering a prolate spheroid accelerating in the fluid [23], [52].

The robotic fish drag and lift coefficients, C_D, C_L, and C_M, are empirically identified using the data collected when the robotic fish is equipped with rigid joints for the pectoral fins. With the rigid joints, the power stroke and recovery stroke need to have different fin speeds, in order to produce a net thrust [38]. This ratio is denoted as $\frac{P}{R}$ ($\frac{\text{Power stroke speed}}{\text{Recovery stroke speed}}$), which is equal to 1 for the symmetric fin-beating pattern. In this paper, experiments are conducted for the cases of $\frac{P}{R} = 2$, 3, 4, and 5. The experimental results for both forward and turning swimming motions of the robotic fish with $\frac{P}{R} = 2$ are used in the body parameter identification. Turning is realized by actuating one pectoral fin only. In particular, these parameters are tuned to match the forward velocity, turning radius, and turning period obtained in simulation with the experimental measurement when two different power stroke speeds are used, completing the power stroke in 0.5 and 0.3 s, respectively. The fin-beat amplitude is set to $\gamma_A = 25^\circ$. The resulting coefficients are $C_D = 0.42$, $C_L = 4.86$, and $C_M = 7.6 \times 10^{-4}$ Kg/m^2. These parameters are then used in independent model validation for all other cases using the flexible rowing joint.

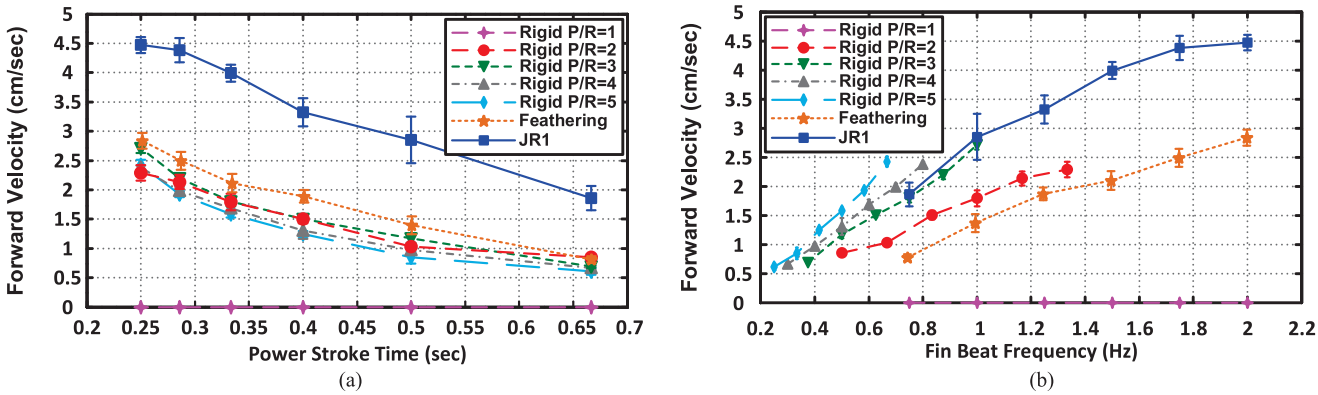

Fig. 9. Experimental results of the forward swimming velocity versus (a) power stroke time, and (b) effective actuation frequency, for the cases of rigid joint and flexible rowing joint.

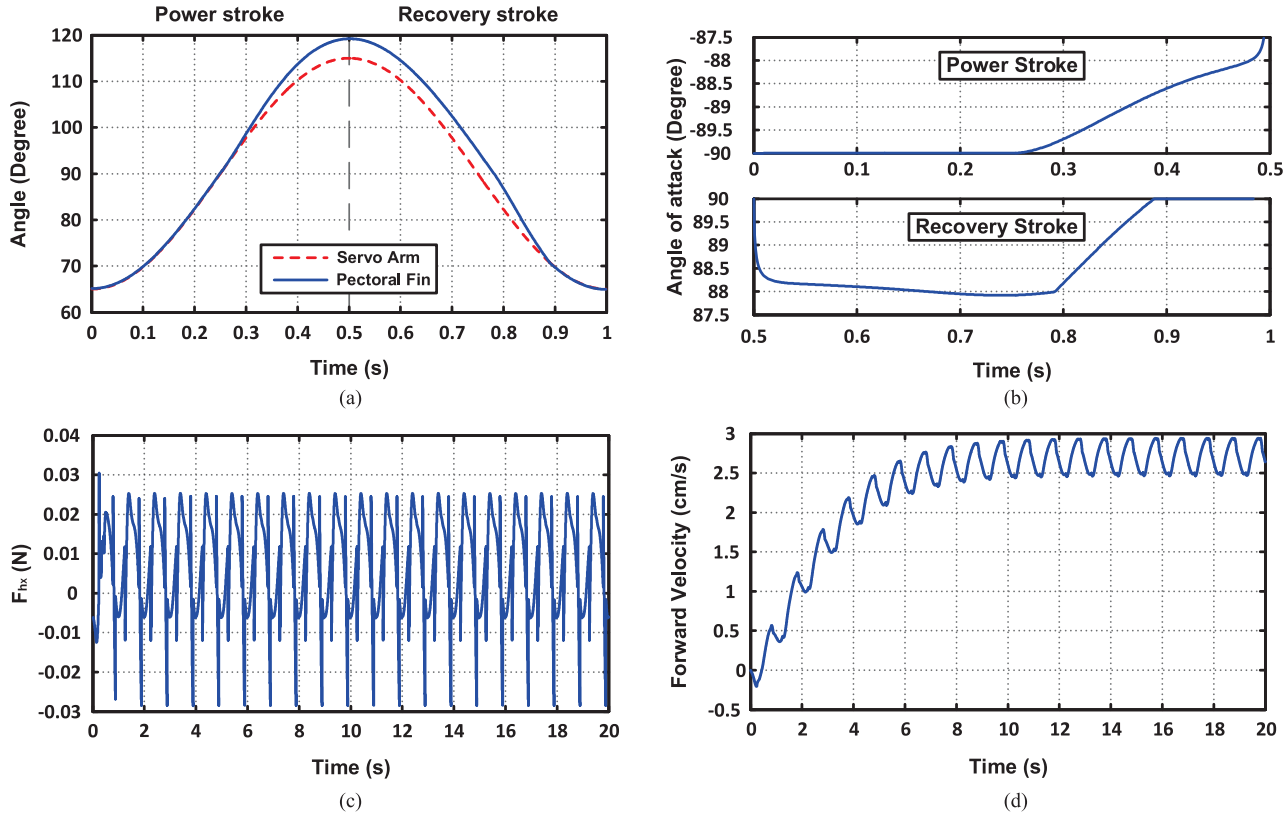

Fig. 10. With fin-beat frequency of 1 Hz: (a) Variation of the pectoral fin and servo arm angle for one movement cycle, (b) Variation of the pectoral fin angle of attack for one movement cycle, (c) Variation of the total hydrodynamic force exerted to robotic fish body in x-direction (F_{h_x}) versus simulation time, (d) Variation of robotic fish velocity in x-direction (V_{C_x}) versus simulation time.

Among all the rowing joints mentioned in Table I, joint "JR1" results in the highest forward velocity. Without the loss of generality, this case is chosen to illustrate the model validation performance. To identify the spring and damper coefficients, K_S and K_D are tuned to match the forward swimming velocity of the robotic fish obtained in simulation with the experimental measurements for fin-beat frequencies of 0.75, 1, and 1.5 Hz. The coefficients are identified $K_S = 6.34 \times 10^{-4}$ N·m and $K_D = 9.98 \times 10^{-5}$ N·m·s. These parameters are then used for model validation for various other cases involving the same joint.

C. Comparison Between Flexible and Rigid Joints

Before presenting the model validation results, we first compare the performance of flexible rowing joints with that of a rigid joint (where the pectoral fins are connected to the servos with a rigid connection). For the rigid joint case, we have the

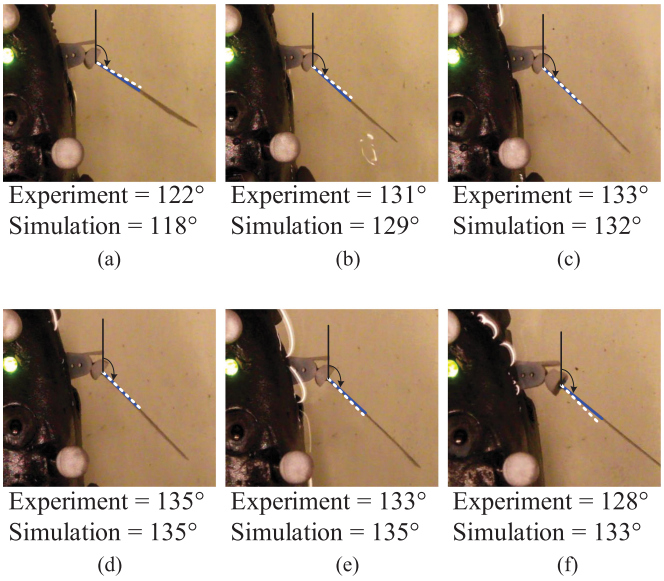

Fig. 11. Comparison between model prediction (white dashed line) and experimental measurement (blue solid line) of the maximum rowing angle during the recovery stroke, with fin-beat frequencies of (a) 0.75, (b) 1, (c) 1.25, (d) 1.5, (e) 1.75, and (f) 2 Hz. The black vertical line indicates the robotic fish heading direction, the green dotted line shows the servo arm direction, and the right pectoral fin is shown.

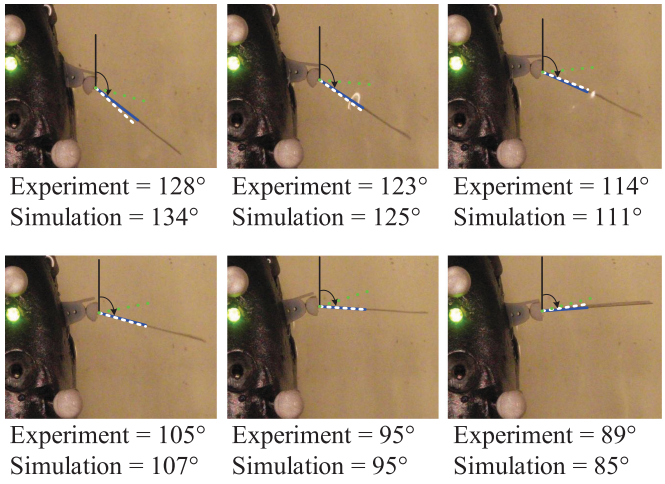

Fig. 12. Comparison between experimental measurements of the time-dependent recovery stroke angle with model predictions. The pectoral fin beats at 1 Hz. The blue solid line and white dashed line imply the experimental measurement and model prediction, respectively, and the green dotted line shows the servo arm direction.

different power and recovery stroke speeds, as mentioned in Section IV-B, so that the robotic fish can have a net thrust.

Fig. 9(a) shows the experimental results on the forward swimming velocities of the rigid joint case with $\frac{P}{R}$= 1, 2, 3, 4, 5, the case of the flexible feathering joint from [53], and the flexible rowing joint JR1, over different power stroke times. Fig. 9(b) presents these results in terms of the effective fin-beat frequencies. The fin-beat frequency means $\frac{1}{T}$, where T denotes the period of each fin-beat cycle (power and recovery stroke combined) and the servos are programed to run up to the limit of 200 °/s. This maximum speed corresponds to the rightmost point in each curve in Fig. 9(b). From Fig. 9, we can conclude that, overall, the velocity performance of the flexible rowing passive joint significantly outperforms the rigid joint case.

D. Dynamic Model Validation

1) Dynamic Characteristics of Pectoral Fins: Before presenting experimental results that validate the dynamic model, we first present simulation results based on the experimentally identified model, to shed insight into the dynamic characteristics of the pectoral fins with flexible joints, as well as their effects on the robotic fish body. In the interest of brevity, we have only included the plots for one case (joint JR1 with fin-beat frequency of 1 Hz, where both fins are actuated). Fig. 10(a) shows the time history of the pectoral fin and servo arm angles in one beat cycle. It is interesting to note that, while the pectoral fin angle follows closely the motor shaft angle during much of the power stroke, the "detachment" starts shortly after the servo passes the 90° during the power stroke, which is due to the inertial effect of the fin when the servo arm starts decelerating. Similarly, the difference between the two angles shrinks down to zero before the recovery stroke ends. Fig. 10(b) shows the angle of attack in power and recovery strokes of one beat cycle, assuming that the robotic fish body is anchored. Fig. 10(c) shows the total force exerted on the body by pectoral fins in the x-direction (F_{h_x}). Note that the mean value of the positive thrust is approximately four times larger than the mean value of negative thrust. The total hydrodynamic force in the y-direction (F_{h_y}) and the total hydrodynamic moment (M_{h_z}) are zero in this case due to the left-right symmetry in paired pectoral fin flapping. Finally, Fig. 10(d) shows the surge velocity of the robotic fish (V_{C_x}) from the simulation. Again, the sway (V_{C_y}) and yaw (ω_{C_z}) components of the robotic fish velocities are zero due to the symmetry in fin-beat flapping. It can be seen that, starting at rest, the robot takes approximately 11 s to reach the steady state.

2) Anchored Experiments: To validate the proposed dynamic model, two sets of experiments are conducted on the robotic fish. During the first set of experiments, the robotic fish body is anchored using a bracket and the angle of the pectoral fin (γ_2) is measured with respect to $\hat{i}$, the robot's heading direction. The motion of the pectoral fin is captured from above, using a Casio Exilim (EX-FH25) high-speed camera at 40 frames/s. Fig. 11 compares the measured maximum values of the rowing angle during the recovery stoke in both simulation and experiments at different fin flapping frequencies, when the robotic fish body is anchored. It can be seen that the model is able to capture the rowing angle well for all frequencies up to 1.75 Hz. For the case of 2 Hz, the noticeable discrepancy between the model prediction and the measurement is likely caused by the constraints in fabrication, were the actual pectoral fin angle goes beyond the servo angle in the power stroke, ($\gamma_1 \neq \gamma_2$), due to the larger hydrodynamic loading on the pectoral fin.

Fig. 12 compares the measured time-dependent pectoral fin angle (γ_2) during the recovery stroke and the corresponding model prediction for the case of 1 Hz actuation. Here, we show the frames every 0.1 s during the recovery stroke. Overall, there is a good match between the model prediction and experimental measurement. The prediction error is slightly larger at the beginning and the end of the cycle, which is attributed to the

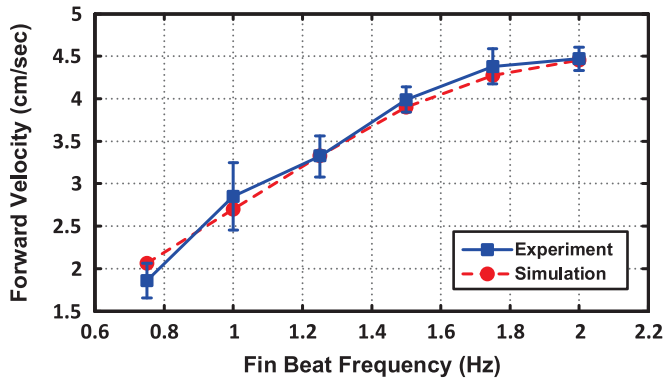

Fig. 13. Case of rowing joint (JR1): Comparison between the model-predicted and measured forward swimming speed, for different fin-beat frequencies.

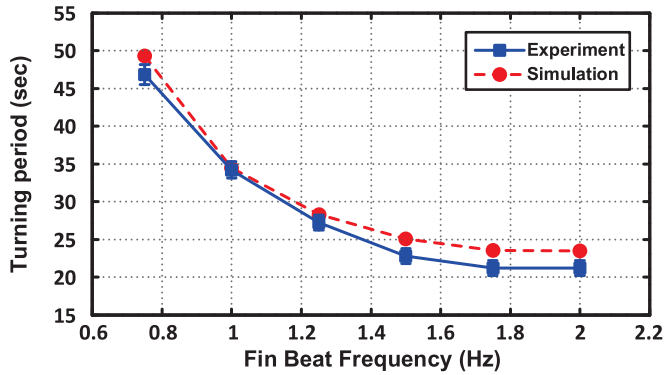

Fig. 14. Case of rowing joint (JR1): Comparison between the model-predicted and measured turning period, for different fin-beat frequencies.

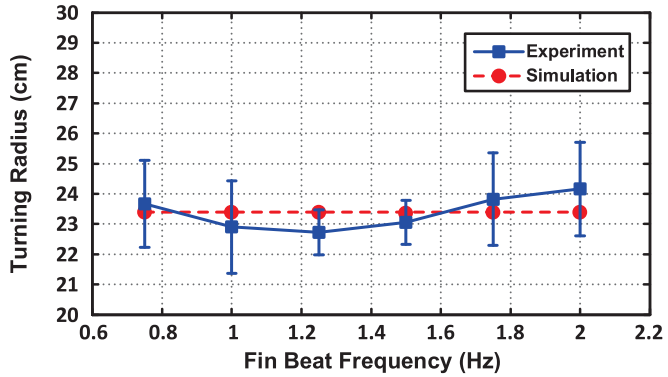

Fig. 15. Case of rowing joint (JR1): Comparison between the model-predicted and measured turning radius for different fin-beat frequencies.

transition from/to the power stroke, where the mechanical stopper is in effect.

3) Free-Swimming Experiments: For the second set of experiments, the robotic fish swims freely in the tank, including both forward swimming and turning that are enabled with the pectoral fins utilizing the flexible rowing joints. Fig. 13 shows the comparison between model prediction and experimental measurement of the forward swim velocity at different fin-beat frequencies. Figs. 14 and 15 show similar comparisons on the turning radius and turning period. From Fig. 14, the turning period drops with the frequency, which is expected. The simulation results in Fig. 15 suggest that the turning radius has negligible dependence on the frequency, which is supported by the experimental results, where the mean values of the measured radius stay around 23–24 cm across all frequencies. The discrepancy between the simulations and experimental results in Fig. 15 is largely attributed to the challenge in measuring precisely the turning radius in experiments—the robot does not track closed orbits for each turn, which could be due to the disturbances from the interactions between the water and tank walls. The results of Figs. 13–15 show that the proposed model is able to capture the motion of the robotic fish with flexible rowing joints very well. In particular, for the tested frequency range, the forward swimming velocity increases with the fin-beat frequency. In the turning case, the turning period (the time it takes to complete one turn) drops with the increasing fin-beat frequency, which matches one's intuition.

V. Effect of Flexible Joint Length and Stiffness

In this section, we investigate the impact of two design parameters for the flexible joint, its length and stiffness, which will allow further validation of the proposed model and demonstrate its potential use for design optimization. As described in [54], the torsional spring constant of a flexible material can be evaluated as

$$K_S = \frac{Edh^3}{12l} \tag{29}$$

where h is the thickness, l is the length, d is the width (depth), and E is the Young's modulus of the flexible material. The damper coefficient K_D can be evaluated as $K_D = \kappa K_S$, where κ is a proportional constant. So the spring constant changes with both dimension and stiffness of the flexible part of the passive joint.

We have chosen three different values for the length of the flexible rowing joint made of FLX980 material, 0.5, 1, and 1.5 mm (Joints JR1, JR2, and JR3 in Table I). The spring and damper constants for JR2 and JR3 are calculated using (29), where the Young's modulus (E) and κ values are kept the same as the ones derived from the parameters K_S and K_D for JR1. Fig. 16 shows the model prediction and experimental results on the forward swimming velocity at different fin-beat frequencies, for all three joints. The joint JR1 has the best performance among the three joints for higher fin-beat frequencies. For lower frequencies (up to 1.25 Hz), joint JR3 (most flexible among the three) has a better performance. We can see that the model is able to effectively capture the joint length-dependence of the forward swimming velocity for all cases. While the experimental limit for the actuation frequency is 2 Hz, we have extended the simulation results to fin-beat frequency of 3 Hz in order to capture the optimal frequency of each joint. The forward swimming speed will drop after reaching this optimal frequency.

Finally, we compare the performance of flexible joints with different material stiffness. Two flexible joints with identical dimensions, JR1 made of FLX980 and JR4 made of DM9850 (stiffer), are used in the comparison. The spring and damper

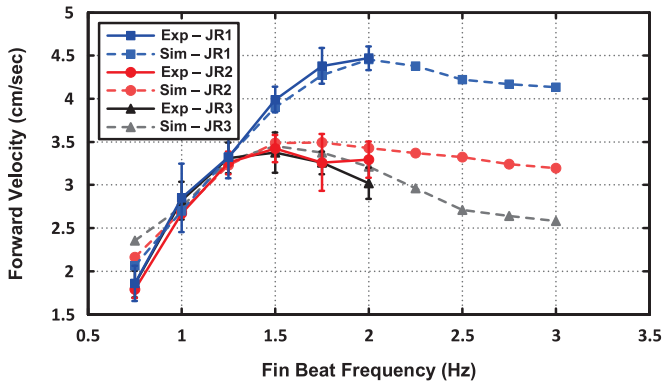

Fig. 16. Model prediction and experimental measurement of the forward swimming velocity of the robotic fish with the use of three flexible joints (all made of FLX980) with different lengths.

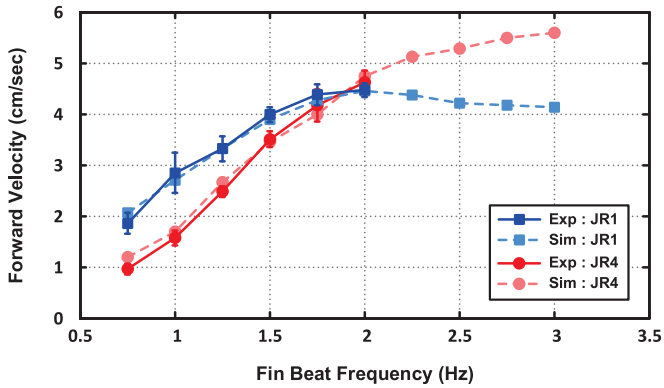

Fig. 17. Model prediction and experimental results of the forward swimming velocity of the robotic fish with the use of two flexible joints with different stiffness values.

coefficients for JR4 are identified to be $K_S = 4.38 \times 10^{-3}$ N·m and $K_D = 9.34 \times 10^{-4}$ N·m·s using the same method described in Section IV-B, and are used for model predictions for all other cases. Fig. 17 shows the comparison of forward swimming speed between the two cases. Again, it can be seen that there is a good match between model predictions and experimental data. For the lower frequencies, the joint JR1 outperforms JR4, while JR4 is the winner for the higher frequencies. Again we have extended the simulation results to higher frequencies to better capture the performance trend of the joints.

VI. Mechanical Efficiency

Robot efficiency, defined as the ratio of useful work for propulsion over total consumed energy, is of great relevance to practical operation of the robot. Mechanical work done by fins to the surrounding water, energy used for powering electronics, electrical losses, and frictional losses, among others, all contributed to the total consumed energy. Mechanical work is arguably the most significant source of energy expenditure, and therefore, it is important to understand how the design of pectoral fin joints influences the mechanical efficiency of the robot. In this section, we use the validated dynamic model to evaluate the propulsive efficiency of the robotic fish swimming with pectoral fins that use the flexible rowing joints. The mechanical efficiency during steady-state swimming is calculated as [3], [35], [55]

$$\eta = \frac{W_b}{W_T} \tag{30}$$

where W_b is the amount of useful work needed to propel the robotic fish and W_T is the total work done by the pectoral fins during each fin-beat cycle. We call this the mechanical efficiency since it does not consider other energy losses, such as the electrical power used for running the electronics or frictional losses in motors and gears. The useful work W_{b_1} can be calculated as

TABLE III
Comparison Between the Two Methods of Computing W_b

Frequency (Hz)	W_{b_1}	W_{b_2}	$\frac{W_{b_1}-W_{b_2}}{W_{b_2}}(\%)$
0.75	0.112	0.114	1.75
1	0.1887	0.1939	2.68
1.25	0.2826	0.2888	2.15
1.5	0.3787	0.3905	3.02
1.75	0.4281	0.4383	2.33
2	0.4233	0.4391	3.6

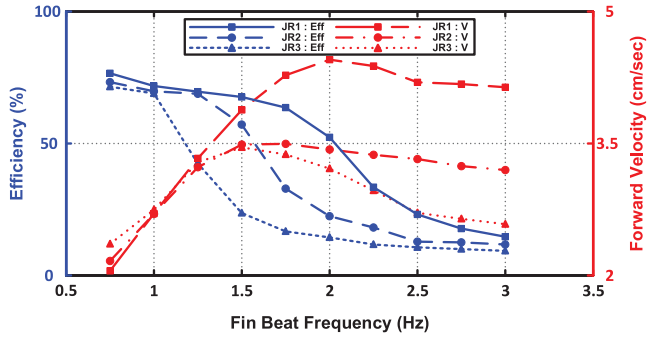

Fig. 18. Calculated mechanical efficiency and forward velocity of different flexible rowing joints at different fin-beat frequencies.

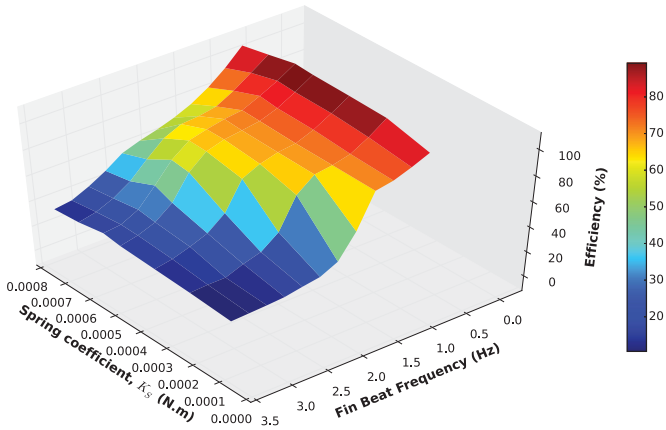

Fig. 19. Calculated mechanical efficiency versus fin-beat frequency and spring constant of the flexible joint.

follows [35], [55]:

$$W_{b_1} = \int_{t_0}^{t_0+T_0} F_{\text{Thrust}}(t) V_C(t) \mathrm{d}t \tag{31}$$

where F_{Thrust} is the x-component of the total fin-generated hydrodynamic force exerted on the robotic fish body (F_{h_x}), $V_C(t)$ is the velocity of the robotic fish body projected into the x-direction, and T_0 denote the total duration of each fin-beat cycle. In this paper, we take an alternative approach that uses product of the mean thrust and the mean velocity at the steady state. When the robotic fish is at the steady state and cruises with a constant speed $V_{C_{\text{mean}}}$, its mean thrust is balanced by its (mean) drag force, and thus

$$F_T = \frac{1}{2}\rho V_{C_{\text{mean}}}^2 S_A C_D \tag{32}$$

which results in the following expression of W_{b_2}:

$$W_{b_2} = \frac{1}{2}\rho V_{C_{\text{mean}}}^3 S_A C_D T_0. \tag{33}$$

As shown in Table III, the values of W_b computed with these two methods are actually very close to each other (with error less than 4%). Given that the second method of evaluating W_{b_2} ignores the oscillatory nature of the thrust and velocity and is thus simpler, it is adopted in the efficiency analysis for the remainder of this paper.

The total work done by the paired pectoral fins, W_T, is obtained as

$$\begin{aligned} W_T &= 2\int_{t_0}^{t_0+T_0} \max\left\{0, \int_0^S \mathrm{d}F_n(s,t)\cdot\vec{v}_p(s,t)\right\}\mathrm{d}t \\ &= 2\int_{t_0}^{t_0+T_0} \max\left\{0, \int_0^S \frac{1}{2}C_n\rho C|\vec{v}_p(s,t)|^2\cdot\vec{v}_p(s,t)\mathrm{d}s\right\}\mathrm{d}t \end{aligned} \tag{34}$$

where t_0 represents the beginning of a fin-beat cycle, "$\cdot$" denotes the inner product. Note that at some time instants t, the instantaneous mechanical power exerted by pectoral fins on water could be negative; however, since the servos cannot reclaim this energy from water, we treat the instantaneous power at such a t as zero, which explains the operator $\max\{0,\cdot\}$ in (34). Note that even at the steady state, the actual velocity is not a constant; instead, it periodically fluctuates around some value. Therefore, $V_{C_{\text{mean}}}$ in (32) is evaluated by the distance traveled over N cycles ($N = 10$) divided by NT_0.

Fig. 18 shows the calculated efficiency, along with the corresponding swimming velocity, for the joints JR1, JR2, and JR3. The efficiency of the joint JR1 is higher than the other two and overall the efficiency is higher for lower fin-beat frequencies. Fig. 18 reveals interesting tradeoff between the speed performance and mechanical efficiency. In particular, for a given joint design, with a higher frequency, the speed is higher but at the cost of lower efficiency. Fig. 19 shows the efficiency curve versus different fin-beat frequencies and spring constant values (k_S). This figure shows that the robotic fish performs more efficiently in lower fin-beat frequencies with stiffer flexible rowing joints up to a certain optimal stiffness ($K_S \approx 7\times10^{-4}$ N·m). For any joint stiffer or more flexible than this optimal amount, the efficiency starts to drop. Overall, Figs. 18 and 19 indicate that the optimization of the flexible joint presents an interesting, multiobjective design problem that involves consideration of the joint stiffness, dimension, and the frequency of fin operation. The proposed dynamic model in this paper shows promise in addressing the optimal design problem.

TABLE IV
COMPARISON OF NONDIMENSIONALIZED PARAMETERS

Robotic fish	St	Re	V_{DL}
This work - JR1	1.27	4273	0.19
This work - JR2	1.35	4044	0.18
This work - JR3	1.32	4116	0.183
[34] with $\gamma_A = 30^\circ$	2.95	5925	0.042
[34] with $\gamma_A = 45^\circ$	2.96	8737	0.0621
[34] with $\gamma_A = 60^\circ$	7.76	4350	0.031
[38]	6.05	900	0.04
[53] - JF1	2.55	1744	0.078
[18]	0.94	10 000	0.16

Fig. 20 provides a comparison of the nondimensionalized parameters for joints JR1, JR2, and JR3 at different fin-beat frequencies. The nondimensionalized parameters considered include the Reynolds number Re, the Strouhal number St, and the dimensionless velocity V_{DL}. Recall the Reynolds number $\text{Re} = \frac{V_{C_{\text{mean}}} L}{\nu}$, where $V_{C_{\text{mean}}}$ is the swimming speed of the robot, L is the robotic fish length, and ν is the kinematic viscosity of water. The robotic fish length $L = 0.15$ m and $\nu = 10^{-6}$ m^2/s are used in the calculation. The Strouhal number is defined as $\text{St} = \frac{fA}{V_{C_{\text{mean}}}}$, where f is the fin-beat frequency, A is the maximum excursion of the trailing edge for pectoral fin, and $V_{C_{\text{mean}}}$ is the swimming speed of the robot. We use $A = 2S\sin\gamma_A$, where S is the pectoral fin span length and γ_A is the fin flapping amplitude [19], [34]. The dimensionless velocity is defined as $V_{\text{DL}} = \frac{V_{C_{\text{mean}}}}{fL}$ [56].

It can be seen in Fig. 20(a) that the efficiency shows clear inverse correlation with the Strouhal number. For example, JR1 demonstrates the highest mechanical efficiency among the three joints and has the lowest Strouhal number. For each joint, the Strouhal number increases while the efficiency drops when the frequency increases. Note that the Strouhal numbers for biological fish are usually in the range of 0.25–0.5 [5], [34], [57]. The Strouhal numbers presented here are higher than 1, and thus, beyond the biological range. The reason is that the robotic fish used in this study is propelled purely by the pectoral fins, which results in low speeds and higher Strouhal numbers. Note that, from Fig. 20(a), when the efficiency of the robotic fish gets higher, the Strouhal number gets closer to the biological range. On the other hand, Fig. 20(b) shows that the robotic fish demonstrates the highest dimensionless velocity when the Reynolds number is at the lower end. Comparing Fig. 20(a) and (b) also suggests that there is a positive (negative, resp.) correlation between the mechanical efficiency (the Strouhal number, resp.) and the dimensionless velocity, which is expected given the definitions of the Strouhal number and the dimensionless velocity.

We have also compared our results with the results (all actuated at 1 Hz) from several pectoral fin-actuated robotic fish reported in the literature, as seen in Table IV. From the table, it can be seen that the Strouhal numbers achieved in this study are

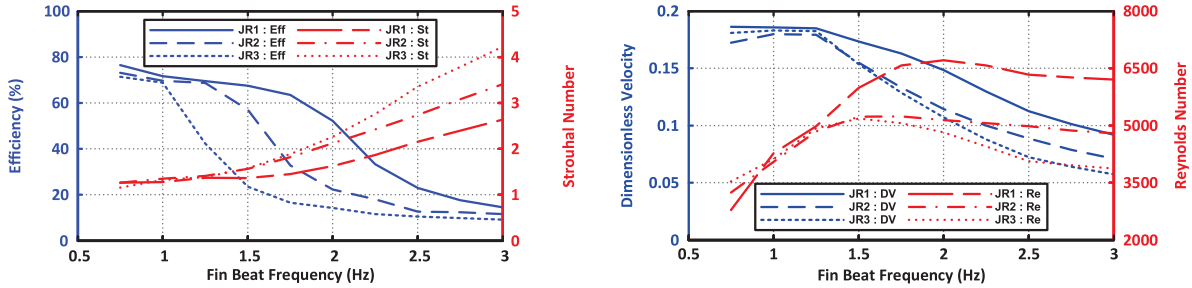

Fig. 20. Comparison of nondimensionalized parameters for joints JR1, JR2, and JR3 at different fin-beat frequencies: (a) Calculated mechanical efficiency and Strouhal number, (b) Dimensionless velocity and Reynolds number.

generally closer to the biological range than what was achieved in other reported work (with the exception of [18], which is slightly lower than our results). The dimensionless velocities achieved in this study are also the highest among all cases. These comparisons provide strong support for the effectiveness of the proposed approach.

VII. Conclusion and Future Work

While biological fish use sophisticated pectoral fin kinematics to achieve superior swimming and maneuvering performance [58], [59], the goal of this study is to achieve sound performance for robotic fish pectoral fins with simple structure and simple control. In particular, we have proposed a novel flexible, passive joint for rowing pectoral fins in robotic fish, and presented a dynamic model for the robotic fish equipped with such pectoral fin mechanisms. The flexible joint enables the pectoral fin to bend back passively along the fish body during the recovery stroke, to minimize the drag force, while maintaining the prescribed motion of the actuator during the power stroke. This design eliminates the need to have different actuation speeds for power and recovery strokes. The blade element theory is used to evaluate the hydrodynamic forces on the pectoral fins. The flexible joint is modeled as a pair of torsional spring and damper. To validate the dynamic model, we have conducted experiments involving both a configuration where the robotic fish is anchored and the fin bending angles are measured, and a free-swimming configuration, where forward swimming speeds and turning radii/periods at different fin-beat frequencies are measured. The performance of the proposed joint is also compared with a traditional rigid joint, to show the effectiveness of this design. Multiple flexible rowing joints are used in the experiments to examine the influence of the flexible joint's length and stiffness on the robotic fish performance, and the experimental data match the model predictions well in all cases, which further supports the utility of the presented model in design optimization. Finally, with the aforementioned model, we have numerically evaluated the mechanical efficiency of the robotic fish and explore its dependence on the flexible joint stiffness and the operating frequency.

There are several directions in which the current work will be extended. First, in this paper, the main focus was to study the performance of flexible rowing joints, so all the studies were done on a rigid, rectangular pectoral fin. The design and prototyping of this joint can be improved, so that collapsing of the fin during the recovery stroke takes place with higher angles (namely, pectoral fin becomes more parallel to the body). Also, it is of interest to extend this study to flexible pectoral fins of different shapes and sizes, which will result in a more complicated hydrodynamic force calculation compared to the current study. We are also interested in the interaction of the caudal fin and the pectoral fins. In particular, the actuation with both pectoral and caudal fins will result in a relatively high velocity for the robotic fish body. As a result, the angle of attack for pectoral fins will no longer be close to 90° and the span-wise component of the pectoral fin force needs to be incorporated.

In the authors' recent work [53], [60], an alternative design of flexible joints for pectoral fins was proposed, where the fin would undergo a passive feathering motion during the recovery stroke. Complementary to the current study, the passive feathering joint represents a more bio-inspired behavior and presents new modeling challenges due to the out-of-plane force component during the feathering phase. On the other hand, experimental results have suggested that the robot tends to show better performance with the rowing joints presented in this study than with the feathering joints. For example, a higher swimming speed is achieved with the rowing joint under the same fin-beat frequency and amplitude. The rowing joint also seems to be able to drive a larger fin. However, it is unclear whether these observations hold true in general or are merely consequences of specific experimental prototypes. Therefore, it is of interest to conduct a more thorough modeling and experimental comparison on these two approaches, to reveal the intrinsic tradeoffs in flexible joint design. Another interesting research direction will be to explore the interaction between the flexible caudal fin and the pectoral fins, in which case the caudal fin can be considered as a propulsion source to enable a higher swimming speed, while the pectoral fins are used for accurate steering and turning.

Acknowledgment

The authors would like to thank John Thon for his contribution to the assembly of the robotic fish prototype and Prof. Philip McKinley for valuable discussions on this paper.

REFERENCES

[1] P. W. Webb, "Hydrodynamics and energetics of fish propulsion," Dept. Environ., Fisheries and Marine Service, Ottawa, ON, Canada, 1975.

[2] S. Childress, *Mechanics of Swimming and Flying* (Cambridge Studies in Mathematical Biology (Book 2)), 1st ed. Cambridge, U.K.: Cambridge Univ. Press, Jul. 1981.

[3] R. Blake, *Fish Locomotion*. Cambridge, U.K.: Cambridge Univ. Press, Jul. 1983.

[4] M. Sfakiotakis, D. M. Lane, and J. B. C. Davies, "Review of fish swimming modes for aquatic locomotion," *IEEE J. Ocean. Eng.*, vol. 24, no. 2, pp. 237–252, Apr. 1999.

[5] M. S. Triantafyllou and G. S. Triantafyllou, "An efficient swimming machine," *Sci. Amer.*, vol. 272, no. 3, pp. 64–71, 1995.

[6] P. V. y. Alvarado and K. Youcef-Toumi, "Design of machines with compliant bodies for biomimetic locomotion in liquid environments," *J. Dyn. Syst., Meas., Control*, vol. 128, no. 1, pp. 3–13, 2005.

[7] T. Ichiklzaki and I. Yamamoto, "Development of robotic fish with various swimming functions," in *Proc. Symp. Underwater Technol. Workshop Sci. Use Submar. Cables Relat. Technol.*, Tokyo, Japan, Apr. 2007, pp. 378–383.

[8] J. Yu, R. Ding, Q. Yang, M. Tan, W. Wang, and J. Zhang, "On a bio-inspired amphibious robot capable of multimodal motion," *IEEE/ASME Trans. Mechatronics*, vol. 17, no. 5, pp. 847–856, Oct. 2012.

[9] J. M. Anderson, K. Streitlien, D. S. Barrett, and M. S. Triantafyllou, "Oscillating foils of high propulsive efficiency," *J. Fluid Mech.*, vol. 360, pp. 41–72, 1998.

[10] X. Tan, "Autonomous robotic fish as mobile sensor platforms: Challenges and potential solutions," *Mar. Technol. Soc. J.*, vol. 45, no. 4, pp. 31–40, 2011.

[11] F. Zhang, O. Ennasr, E. Litchman, and X. Tan, "Autonomous sampling of water columns using gliding robotic fish: Algorithms and harmful algae-sampling experiments," *IEEE Syst. J.*, vol. 10, no. 3, pp. 1271–1281, 2016.

[12] S. Marras and M. Porfiri, "Fish and robots swimming together: Attraction towards the robot demands biomimetic locomotion," *J. Roy. Soc. Interface*, vol. 9, no. 73, pp. 1856–1868, 2012.

[13] R. Mason and J. Burdick, "Construction and modelling of a carangiform robotic fish," in *Proc. 6th Int. Symp. Exp. Robot. VI*, Jan. 2000, vol. 250, pp. 235–242.

[14] J. M. Anderson and N. K. Chhabra, "Maneuvering and stability performance of a robotic tuna," *Integr. Comp. Biol.*, vol. 42, no. 1, pp. 118–126, 2002.

[15] K. H. Low, "Locomotion and depth control of robotic fish with modular undulating fins," *Int. J. Autom. Comput.*, vol. 3, no. 4, pp. 348–357, 2006.

[16] J. D. Liu and H. Hu, "Biologically inspired behaviour design for autonomous robotic fish," *Int. J. Automat. Comput.*, vol. 3, no. 4, pp. 336–347, 2006.

[17] J. Wang and X. Tan, "Averaging tail-actuated robotic fish dynamics through force and moment scaling," *IEEE Trans. Robot.*, vol. 31, no. 4, pp. 906–917, Aug. 2015.

[18] D. Lachat, A. Crespi, and A. Ijspeert, "BoxyBot: A swimming and crawling fish robot controlled by a central pattern generator," in *Proc. 1st IEEE/RAS-EMBS Int. Conf. Biomed. Robot. Biomechatronics*, Pisa, Italy, Feb. 2006, pp. 643–648.

[19] P. Kodati, J. Hinkle, A. Winn, and X. Deng, "Microautonomous robotic ostraciiform (MARCO): Hydrodynamics, design and fabrication," *IEEE Trans. Robot.*, vol. 24, no. 1, pp. 105–117, Feb. 2008.

[20] J. Wang and X. Tan, "A dynamic model for tail-actuated robotic fish with drag coefficient adaptation," *Mechatronics*, vol. 23, no. 6, pp. 659–668, 2013.

[21] X. Deng and S. Avadhanula, "Biomimetic micro underwater vehicle with oscillating fin propulsion: System design and force measurement," in *Proc. IEEE Int. Conf. Robot. Autom.*, Barcelona, Spain, Apr. 2005, pp. 3312–3317.

[22] Z. Wang, G. Hang, J. Li, Y. Wang, and K. Xiao, "A micro-robot fish with embedded SMA wire actuated flexible biomimetic fin," *Sens. Actuators A, Phys.*, vol. 144, no. 2, pp. 354–360, 2008.

[23] M. Aureli, V. Kopman, and M. Porfiri, "Free-locomotion of underwater vehicles actuated by ionic polymer metal composites," *IEEE/ASME Trans. Mechatronics*, vol. 15, no. 4, pp. 603–614, Aug. 2010.

[24] Z. Chen, S. Shatara, and X. Tan, "Modeling of biomimetic robotic fish propelled by an ionic polymer-metal composite caudal fin," *IEEE/ASME Trans. Mechatronics*, vol. 15, no. 3, pp. 448–459, Jun. 2010.

[25] Z. Chen, T. I. Um, J. Zhu, and H. Bart-Smith, "Bio-inspired robotic cownose ray propelled by electroactive polymer pectoral fin," in *Proc. ASME Int. Mech. Eng. Congr. Expo.*, Denver, CO, USA, Nov. 2011, vol. 2, pp. 817–824.

[26] S. Kobayashi, M. Nakabayashi, and H. Morikawa, "Bioinspired propulsion mechanism in fluid using fin with dynamic variable-effective-length spring," *J. Biomech. Sci. Eng.*, vol. 1, no. 1, pp. 280–289, 2006.

[27] J. H. Long Jr *et al.*, "Biomimetic evolutionary analysis: Testing the adaptive value of vertebrate tail stiffness in autonomous swimming robots," *J. Exp. Biol.*, vol. 209, no. 23, pp. 4732–4746, 2006.

[28] M. Ziegler and R. Pfeifer, "Sensory feedback of a fish robot with tunable elastic tail fin," in *Proc. 2nd Int. Conf. Biomimetic Biohybrid Syst.*, 2013, vol. 8064, pp. 335–346.

[29] Y.-J. Park, T. M. Huh, D. Park, and K.-J. Cho, "Design of a variable-stiffness flapping mechanism for maximizing the thrust of a bio-inspired underwater robot," *Bioinspir. Biomim.*, vol. 9, no. 3, 2014, Art. no. 036002.

[30] S. Bazaz Behbahani and X. Tan, "Dynamic modeling of robotic fish caudal fin with electrorheological fluid-enabled tunable stiffness," in *Proc. ASME Dynamic Syst. Control Conf.*, Columbus, OH, USA, Oct. 2015, vol. 3, p. V003T49A006.

[31] K. A. Morgansen, B. I. Triplett, and D. J. Klein, "Geometric methods for modeling and control of free-swimming fin-actuated underwater vehicles," *IEEE Trans. Robot.*, vol. 23, no. 6, pp. 1184–1199, Dec. 2007.

[32] N. Kato and M. Furushima, "Pectoral fin model for maneuver of underwater vehicles," in *Proc. Symp. Auton. Underwater Veh. Technol.*, Monterey, CA, USA, Jun. 1996, pp. 49–56.

[33] N. Kato, B. Wicaksono, and Y. Suzuki, "Development of biology-inspired autonomous underwater vehicle BASS III with high maneuverability," in *Proc. Int. Symp. Underwater Technol.*, Tokyo, Japan, May 2000, pp. 84–89.

[34] P. E. Sitorus, Y. Y. Nazaruddin, E. Leksono, and A. Budiyono, "Design and implementation of paired pectoral fins locomotion of labriform fish applied to a fish robot," *J. Bionic Eng.*, vol. 6, no. 1, pp. 37–45, 2009.

[35] H. Suzuki, N. Kato, and K. Suzumori, "Load characteristics of mechanical pectoral fin," *Exp. Fluids*, vol. 44, no. 5, pp. 759–771, 2008.

[36] N. Kato *et al.*, "Elastic pectoral fin actuators for biomimetic underwater vehicles," in *Bio-Mechanisms of Swimming and Flying*, N. Kato and S. Kamimura, Eds. New York, NY, USA: Springer, Jan. 2008, pp. 271–282.

[37] J. Palmisano, R. Ramamurti, K.-J. Lu, J. Cohen, W. Sandberg, and B. Ratna, "Design of a biomimetic controlled-curvature robotic pectoral fin," in *Proc. IEEE Int. Conf. Robot. Autom.*, Rome, Italy, Apr. 2007, pp. 966–973.

[38] S. Bazaz Behbahani, J. Wang, and X. Tan, "A dynamic model for robotic fish with flexible pectoral fins," in *Proc. IEEE/ASME Int. Conf. Adv. Intell. Mechatronics*, Wollongong, Australia, Jul. 2013, pp. 1552–1557.

[39] C. Phelan, J. Tangorra, G. Lauder, and M. Hale, "A biorobotic model of the sunfish pectoral fin for investigations of fin sensorimotor control," *Bioinspir. Biomim.*, vol. 5, no. 3, 2010, Art. no. 035003.

[40] W. Wang and G. Xie, "CPG-based locomotion controller design for a boxfish-like robot," *Int. J. Adv. Robot. Syst.*, vol. 11, no. 87, pp. 1–11, 2014.

[41] A. Crespi, D. Lachat, A. Pasquier, and A. Ijspeert, "Controlling swimming and crawling in a fish robot using a central pattern generator," *Auton. Robots*, vol. 25, nos. 1/2, pp. 3–13, 2008.

[42] J. Gao, S. Bi, Y. Xu, and C. Liu, "Development and design of a robotic manta ray featuring flexible pectoral fins," in *Proc. IEEE Int. Conf. Robot. Biomimetics*, Sanya, China, Dec. 2007, pp. 519–523.

[43] Z. Chen, T. Um, and H. Bart-Smith, "Bio-inspired robotic manta ray powered by ionic polymer-metal composite artificial muscles," *Int. J. Smart Nano Mater.*, vol. 3, no. 4, pp. 296–308, 2012.

[44] N. Kato, "Control performance in the horizontal plane of a fish robot with mechanical pectoral fins," *IEEE J. Ocean. Eng.*, vol. 25, no. 1, pp. 121–129, Jan. 2000.

[45] S. Bazaz Behbahani and X. Tan, "A flexible passive joint for robotic fish pectoral fins: Design, dynamic modeling, and experimental results," in *Proc. IEEE/RSJ Int. Conf. Intell. Robots Syst.*, Chicago, IL, USA, Sep. 2014, pp. 2832–2838.

[46] G. Barbera, L. Pi, and X. Deng, "Attitude control for a pectoral fin actuated bio-inspired robotic fish," in *Proc. IEEE Int. Conf. Robot. Autom.*, Shanghai, China, May 2011, pp. 526–531.

[47] G. Barbera, "Theoretical and experimental analysis of a control system for a vehicle biomimetic 'boxfish'," M.S. thesis, Dept. Inform. Eng., Univ. of Padua, Padua, Italy, 2008.
[48] J. Wang, P. K. McKinley, and X. Tan, "Dynamic modeling of robotic fish with a base-actuated flexible tail," *J. Dyn. Syst., Meas., Control*, vol. 137, no. 1, 2015, Art. no. 011004.
[49] E. G. Drucker, J. A. Walker, and M. W. Westneat, "Mechanics of pectoral fin swimming in fishes," *Fish Physiol.*, vol. 23, pp. 369–423, 2005.
[50] R. Dong, *Effective Mass and Damping of Submerged Structures*. Dept. of Energy, Washington, DC, USA, 1978.
[51] V. Kopman and M. Porfiri, "Design, modeling, and characterization of a miniature robotic fish for research and education in biomimetics and bioinspiration," *IEEE/ASME Trans. Mechatronics*, vol. 18, no. 2, pp. 471–483, Apr. 2013.
[52] T. I. Fossen, *Guidance and Control of Ocean Vehicles*. New York, NY, USA: Wiley, 1994.
[53] S. Bazaz Behbahani and X. Tan, "Bio-inspired flexible joints with passive feathering for robotic fish pectoral fins," *Bioinspir. Biomim.*, vol. 11, no. 3, 2016, Art. no. 036009.
[54] A. Banerjee and S. Nagarajan, "Efficient simulation of large overall motion of beams undergoing large deflection," *Multibody Syst. Dyn.*, vol. 1, no. 1, pp. 113–126, 1997.
[55] M. Nakashima, N. Ohgishi, and K. Ono, "A study on the propulsive mechanism of a double jointed fish robot utilizing self-excitation control," *JSME Int. J. Ser. C*, vol. 46, pp. 982–990, 2003.
[56] J. J. Videler and F. Hess, "Fast continuous swimming of two pelagic predators, saithe (pollachius virens) and mackerel (scomber scombrus): A kinematic analysis," *J. Exp. Biol.*, vol. 109, no. 1, pp. 209–228, 1984.
[57] J. J. Rohr and F. E. Fish, "Strouhal numbers and optimization of swimming by odontocete cetaceans," *J. Exp. Biol.*, vol. 207, no. 10, pp. 1633–1642, 2004.
[58] M. E. Hale, R. D. Day, D. H. Thorsen, and M. W. Westneat, "Pectoral fin coordination and gait transitions in steadily swimming juvenile reef fishes," *J. Exp. Biol.*, vol. 209, no. 19, pp. 3708–3718, 2006.
[59] G. V. Lauder and J. L. Tangorra, "Fish locomotion: Biology and robotics of body and fin-based movements," in *Robot Fish: Bio-Inspired Fishlike Underwater Robots*. Berlin, Germany: Springer, 2015, pp. 25–49.
[60] S. Bazaz Behbahani and X. Tan, "Design and dynamic modeling of a flexible feathering joint for robotic fish pectoral fins," in *Proc. ASME Dynamic Syst. Control Conf.*, San Antonio, TX, USA, Oct. 2014, vol. 1, p. V001T05A005 (9 pages).

Sanaz Bazaz Behbahani (S'14) received the B.S. degree in electrical engineering from Amir Kabir University of Technology (Tehran Polytechnic), Tehran, Iran, in 2008. She is currently working toward the Ph.D. degree in the Smart Microsystems Laboratory, Department of Electrical and Computer Engineering, Michigan State University, East Lansing, MI, USA.

Her Ph.D. thesis is mainly focused on investigating the role of flexibility in robotic fish, where she has designed and developed fish-like robots from the initial concept, through system modeling, control, and finally prototyping. Her research interests include mechatronics, robotics, soft robots, modeling, and control theory.

Dr. Bazaz Behbahani was a finalist for the Best Student Paper Award in ASME 2014 Dynamic Systems and Control Conference, and her article was featured in *Bioinspiration & Biomimetics* in 2016.

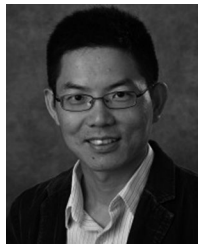

Xiaobo Tan (S'97–M'02–SM'11) received the B.Eng. and M.Eng. degrees in automatic control from Tsinghua University, Beijing, China, in 1995 and 1998, respectively, and the Ph.D. degree in electrical and computer engineering from University of Maryland, College Park, MD, USA, in 2002.

From September 2002 to July 2004, he was a Research Associate with Institute for Systems Research, University of Maryland. He joined the Faculty of the Department of Electrical and Computer Engineering, Michigan State University (MSU), East Lansing, MI, USA, in 2004, where he is currently an MSU Foundation Professor. His research interests include bio-inspired underwater robots, mobile sensing in aquatic environments, soft sensing and actuation materials, and modeling and control of systems with hysteresis. He has coauthored one book, which is entitled *Biomimetic Robotic Artificial Muscles* (World Scientific, 2013) and more than 80 journal papers, and holds one US patent.

Dr. Tan has served as an Associate Editor/Technical Editor for *Automatica*, IEEE/ASME TRANSACTIONS ON MECHATRONICS, and *International Journal of Advanced Robotic Systems*. He served as the Program Chair of the 2011 International Conference on Advanced Robotics, and the Finance Chair of the 2015 American Control Conference. He received the NSF CAREER Award (2006), MSU Teacher-Scholar Award (2010), and several best paper awards.